Electr Eng
DOI 10.1007/s00202-017-0554-y

ORIGINAL PAPER

Implementation and experimental investigation of a sensorless field-oriented control scheme for permanent-magnet synchronous generators

Mohamed Abdelrahem[1,2] · **Christoph Michael Hackl**[3] · **Ralph Kennel**[1]

Received: 25 January 2017 / Accepted: 1 May 2017

Abstract Variable-speed wind energy conversion systems based on permanent-magnet synchronous generators (PMSGs) are typically controlled using the field-oriented control (FOC) principles. Therefore, accurate information of the rotor speed and position are essential to perform the required reference frame transformations. These signals can be obtained by mechanical sensors (e.g., position encoders or speed transducers) or via estimation schemes. This paper proposes a sensorless FOC strategy for direct-driven PMSGs in variable-speed wind turbines. A synchronously rotating reference frame phase-locked loop (PLL) that utilizes a model-based back elector-motive force (back-EMF) estimation is employed to estimate the rotor speed and position of the PMSG. The proposed sensorless FOC strategy is experimentally implemented, and its performance is investigated for all operation conditions and under parameter variations of the PMSG.

✉ Mohamed Abdelrahem
mohamed.abdelrahem@tum.de

Christoph Michael Hackl
christoph.hackl@tum.de
https://www.cres.mse.tum.de

Ralph Kennel
ralph.kennel@tum.de

[1] Institute for Electrical Drive Systems and Power Electronics, Technical University of Munich (TUM), Munich, Germany

[2] Electrical Engineering Department, Faculty of Engineering, Assiut University, Assiut, Egypt

[3] Munich School of Engineering, Research Group "Control of Renewable Energy Systems (CRES)", Technical University of Munich (TUM), Munich, Germany

Keywords Sensorless control · Permanent-magnet synchronous generator · Variable-speed wind turbines · Phase-locked loop · Field-oriented control

1 Introduction

Renewable energy resources are considered as an alternative to conventional electrical power generation due to their advantages of sustainability and environmental friendliness. Among these resources, wind energy is a promising and favorable electrical power generation source. Recently, wind energy conversion systems (WECSs) with permanent-magnet synchronous generators (PMSGs) are becoming more popular in the wind energy industry due to the elimination of the gear box and/or the electrical excitation system. Moreover, WECSs with full power converters allow for a more reliable and simpler low-voltage ride through during faults [1–5]. Generally, the PMSG is controlled according to the field-oriented control (FOC) principle. Thus, incremental encoders and/or speed transducers are utilized for measuring the rotor position and/or speed. However, incremental encoders and/or speed transducers make wiring and precise mounting necessary and, hence, might lead to a reduced reliability. These problems can be avoided by using position sensorless control strategies [6].

Various speed/position sensorless control schemes have been presented for permanent-magnet synchronous machines (PMSMs). An extend Kalman filter (EKF) has been proposed for speed and position estimation of the PMSG in [7–10]. The EKF is an optimal estimator in the least-squares sense. It estimates the states of the dynamic nonlinear system and is robust against parameters variations of the PMSG. However, the high calculation burden is the main disadvantage of the EKF. A model reference adaptive system (MRAS) observer

Published online: 13 May 2017

has been presented in [11–13]. This MRAS observer is simple and easy to implement. However, its sensitivity to parameter variations of the PMSG is its main drawback. A sliding-mode observer (SMO) has been proposed in [14–16]. SMO is robust against parameter variations of the PMSG. However, undesirable deteriorations might occur in the estimated speed due to chattering. Neural network-based observers have been proposed for sensorless control of the PMSG in [17], and an adaptive network-based fuzzy inference system observer has been presented in [18]. These two observers achieve a good estimation performance and are robust against parameter variations of the PMSG. However, the high complexity of both observers is their main drawback.

Phase-locked loops (PLLs) are well-known and crucial in synchronization and control of grid-connected converters/inverters [19]. Furthermore, PLLs have been utilized for sensorless control of induction motors [20] and PMSMs [21]. Recently, PLLs have been proposed for sensorless control of PMSG [22,23]. However, the robustness of the PLL against parameters variations of the PMSG has not been investigated. Furthermore, the output power of the PMSG was kept constant while the rotor speed was varied or the rotor speed was kept constant while the output power of the PMSG was varied, both scenarios do not represent the real dynamics of a variable-speed wind turbine system. In reality, when the wind speed is below the nominal wind speed and is changing, the rotor speed and the output power are varying at the same time.

In this paper, a synchronously rotating reference frame PLL that utilizes the model-based back elector-motive force to estimate the rotor speed and position of the PMSG is presented. The PMSG is controlled according to the FOC strategy. The dynamics of the WECS are considered by varying the output power of the PMSG and the rotor speed at the same time. The proposed sensorless FOC scheme is experimentally validated, and its response is investigated for all the operation conditions and under parameter variations of the PMSG.

This paper is organized as follows: Sect. 2 presents a brief description of the PMSG model and its control. The proposed PLL is presented in Sect. 3. The experimental setup and the experimental results investigating the estimation performance and robustness are discussed in Sect. 4. Finally, the paper is concluded in Sect. 5.

2 Modeling and control of the PMSG

The dynamical model of a three-phase surface-mounted PMSG can be written in the synchronously rotating dq reference frame as follows [24]:

$$\left.\begin{aligned} u_{\mathrm{s}}^{d} &= R_{\mathrm{s}} i_{\mathrm{s}}^{d} + L_{\mathrm{s}} \tfrac{d}{\mathrm{d}t} i_{\mathrm{s}}^{d} - \omega_{\mathrm{r}} L_{\mathrm{s}} i_{\mathrm{s}}^{q} + e_{\mathrm{s}}^{d}, \\ u_{\mathrm{s}}^{q} &= R_{\mathrm{s}} i_{\mathrm{s}}^{q} + L_{\mathrm{s}} \tfrac{d}{\mathrm{d}t} i_{\mathrm{s}}^{q} + \omega_{\mathrm{r}} L_{\mathrm{s}} i_{\mathrm{s}}^{d} + e_{\mathrm{s}}^{q}, \end{aligned}\right\} \tag{1}$$

and

$$\left.\begin{aligned} \tfrac{d}{\mathrm{d}t}\omega_{\mathrm{m}} &= \tfrac{1}{\Theta}(T_{\mathrm{e}} - T_{\mathrm{m}} - \nu\omega_{\mathrm{m}}), \\ T_{\mathrm{e}} &= \tfrac{3}{2} n_{\mathrm{p}} \psi_{\mathrm{pm}} i_{\mathrm{s}}^{q}, \end{aligned}\right\} \tag{2}$$

where $u_{\mathrm{s}}^{d}, u_{\mathrm{s}}^{q}, i_{\mathrm{s}}^{d}, i_{\mathrm{s}}^{q}, e_{\mathrm{s}}^{d}, e_{\mathrm{s}}^{q}$ are the d- and q-axes components of the stator voltage (in V), current (in A), and back elector-motive force (EMF) (in V) of the PMSG, respectively. R_{s} and L_{s} are the stator resistance (in Ω) and inductance (in H) of the PMSG, respectively. $\omega_{\mathrm{r}} = n_{\mathrm{p}}\omega_{\mathrm{m}}$ is the electrical angular speed of the rotor (in rad/s) (n_{p} is the pole pair number, and ω_{m} is the mechanical angular speed of the rotor) and ψ_{pm} is the permanent-magnet flux linkage (in Wb). T_{e} is the electromagnetic torque (in Nm), and T_{m} is the mechanical torque produced by the wind turbine. Θ is the overall rotor inertia (in kg/m^2) of the wind turbine and PMSG, and ν is the viscous friction coefficient (in N m s).

In Fig. 1, a voltage source converter (VSC) is utilized to control the PMSG to accomplish the maximum power point tracking (MPPT). The controller is designed according to the FOC strategy and composed of a current control loop for controlling the d- and q-axes currents of the PMSG, and a MPPT algorithm to compute the optimal torque $T_{\mathrm{e}}^{\star} = -k_{\mathrm{p}}^{\star}\hat{\omega}_{\mathrm{m}}^{2}$ with a positive constant $k_{\mathrm{p}}^{\star}$ [9,24]. This optimal torque is used to compute the q-axis reference current as $i_{\mathrm{s,ref}}^{q} = \frac{2}{3n_{\mathrm{p}}\psi_{\mathrm{pm}}} T_{\mathrm{e}}^{\star}$ while the d-axis reference current $i_{\mathrm{s,ref}}^{d}$ is set to zero. Then, the errors between the reference d- and q-axis currents and the actual ones are processed by PI controllers producing the reference d- and q-axes voltages. Finally, a space vector modulation (SVM) is used to generate the switching signals of the VSC.

The current control loop of the PMSG can be simplified in Laplace domain as shown in Fig. 2 [24]. In this figure, K_{p} and T_{i} are the parameters of the PI controller; T_{d} is the delay time due to the voltage source converter (including also measure-

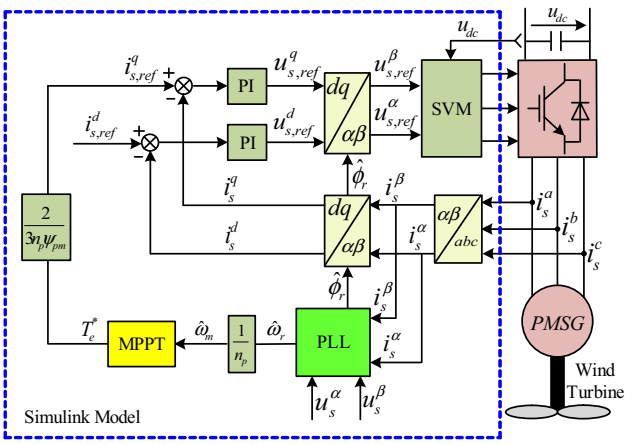

Fig. 1 Sensorless field-oriented control of PMSG in variable-speed WECSs

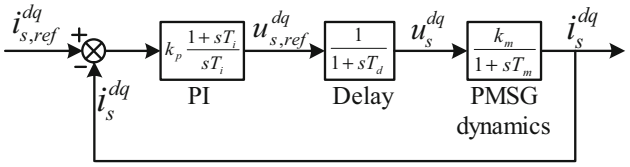

Fig. 2 Schematic diagram of the PMSG current control loop in Laplace domain

ment, signal conditioning, and analog-to-digital conversion); $k_\mathrm{m} = \frac{1}{R_\mathrm{s}}$ and $T_\mathrm{m} = \frac{L_\mathrm{s}}{R_\mathrm{s}}$ are the system gain and stator time constant of the PMSG dynamics. The d and q PI controllers are tuned with help of the Magnitude Optimum method to achieve a fast transient performance [24]. Accordingly, the PI controller parameters are selected as follows:

$$T_i = T_\mathrm{m} \quad \text{and} \quad k_\mathrm{p} = \frac{T_\mathrm{m}}{2k_\mathrm{m}T_\mathrm{d}}. \tag{3}$$

The time delay T_d is selected equal to the sampling time (i.e., $T_\mathrm{d} = T_\mathrm{s}$).

3 Proposed phase-locked loop

Phase-locked loop (PLL) synchronizes its output in frequency as well as in phase with its input. PLLs are now widely utilized for the synchronization of power converters/inverters, sensorless control, and also for monitoring purposes in different engineering fields [19]. Figure 3 illustrates the vector diagram of the permanent-magnet flux-oriented reference frame [22], where ϕ_r and $\hat{\phi}_\mathrm{r}$ are the actual and the estimated rotor position, respectively. The d-axis is expected to be located on the permanent-magnet flux. However, an initial error between ϕ_r and $\hat{\phi}_\mathrm{r}$ (i.e., $\Delta\phi_\mathrm{r} = \phi_\mathrm{r} - \hat{\phi}_\mathrm{r}$) might exist. For small $\Delta\phi_\mathrm{r}$, the EMF component $e_\mathrm{s}^d \approx \Delta\phi_\mathrm{r}$ approximates the angle difference. Therefore, e_s^d can be utilized as an indicator to illustrate whether the d-axis and the permanent-magnet flux are aligned or not. Therefore, estimation of the back-EMF vector $e_\mathrm{s}^{dq} = (e_\mathrm{s}^d, e_\mathrm{s}^q)^\top$ is essential. To do so, a discrete-time model of the PMSG is helpful. For discretization, the forward Euler method with sampling time T_s (in s) is applied to the time-continuous model (1). Accordingly, the discrete-time model of the PMSG can be expressed as follows

$$\left.\begin{aligned} u_\mathrm{s}^d[k] &= R_\mathrm{s} i_\mathrm{s}^d[k] + L_\mathrm{s}\tfrac{i_\mathrm{s}^d[k+1]-i_\mathrm{s}^d[k]}{T_\mathrm{s}} - \omega_\mathrm{r}[k]L_\mathrm{s}i_\mathrm{s}^q[k] \\ &\quad + e_\mathrm{s}^d[k], \\ u_\mathrm{s}^q[k] &= R_\mathrm{s} i_\mathrm{s}^q[k] + L_\mathrm{s}\tfrac{i_\mathrm{s}^q[k+1]-i_\mathrm{s}^q[k]}{T_\mathrm{s}} + \omega_\mathrm{r}[k]L_\mathrm{s}i_\mathrm{s}^d[k] \\ &\quad + e_\mathrm{s}^q[k], \end{aligned}\right\} \tag{4}$$

where k is the current sampling instant. Using (4), e_s^d and e_s^q can be computed as

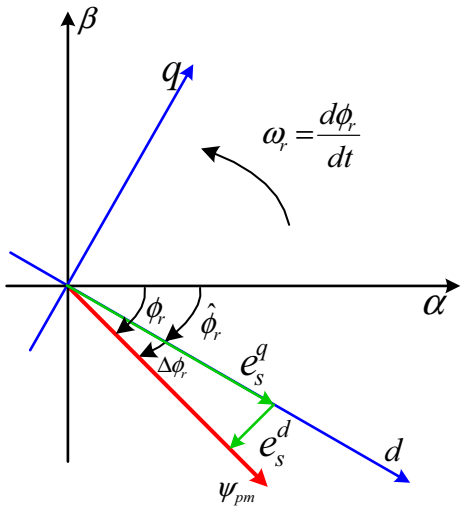

Fig. 3 Vector diagram of the permanent-magnet flux-oriented reference frame

$$\left.\begin{aligned} e_\mathrm{s}^d[k] &= -R_\mathrm{s} i_\mathrm{s}^d[k] - L_\mathrm{s}\tfrac{i_\mathrm{s}^d[k+1]-i_\mathrm{s}^d[k]}{T_\mathrm{s}} + \omega_\mathrm{r}[k]L_\mathrm{s}i_\mathrm{s}^q[k] \\ &\quad + u_\mathrm{s}^d[k], \\ e_\mathrm{s}^q[k] &= -R_\mathrm{s} i_\mathrm{s}^q[k] - L_\mathrm{s}\tfrac{i_\mathrm{s}^q[k+1]-i_\mathrm{s}^q[k]}{T_\mathrm{s}} - \omega_\mathrm{r}[k]L_\mathrm{s}i_\mathrm{s}^d[k] \\ &\quad + u_\mathrm{s}^q[k]. \end{aligned}\right\} \tag{5}$$

With e_s^d as in (5), the proposed PLL can be designed as shown in Fig. 4 [22]. As illustrated in this figure, e_s^d is fed back and compared to its reference $e_\mathrm{s,ref}^d = 0$, while the estimation error $\Delta e_\mathrm{s}^d = e_\mathrm{s,ref}^d - e_\mathrm{s}^d$ is processed by a fixed-gain PI controller to produce the compensation term $\Delta\hat{\omega}$. The q-axis component of the back-EMF e_s^q is utilized to compute the feed-forward term $\hat{\omega}_{ff}$ as follows

$$\hat{\omega}_{ff} = \frac{e_\mathrm{s}^q[k]}{\psi_\mathrm{pm}} \tag{6}$$

to accelerate the estimation process. Then, the estimated rotor speed $\hat{\omega}$ can be expressed as

$$\hat{\omega} = \Delta\hat{\omega} + \hat{\omega}_{ff}. \tag{7}$$

The estimated rotor speed $\hat{\omega}$ needs to be filtered by a low-pass filter (LPF) in order to reduce the effect of high-frequency noise, see Fig. 4. Then, the estimation of the rotor position $\hat{\phi}_\mathrm{r}[k]$ can be achieved by integrating $\hat{\omega}_\mathrm{r}[k]$ as follows

$$\hat{\phi}_\mathrm{r}[k] = \hat{\phi}_\mathrm{r}[k-1] + T_\mathrm{s}\hat{\omega}_\mathrm{r}[k]. \tag{8}$$

The tuning of the PI controller is done according to the rules presented in [21].

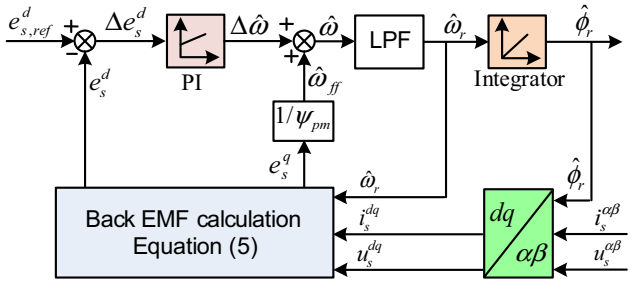

Fig. 4 Schematic diagram of the proposed PLL for sensorless FOC of PMSG

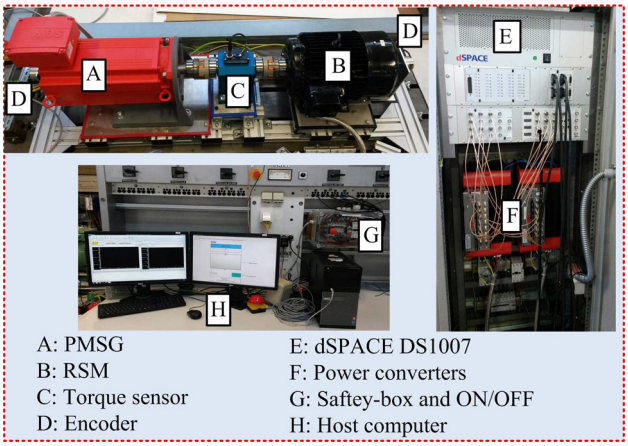

Fig. 5 Constructed test-bench to validate the proposed PLL for sensorless FOC of PMSGs

4 Experimental results and discussion

The proposed PLL is experimentally implemented. The setup consists of a 14.5 kW PMSG driven by a two-level power converter and controlled by a FOC scheme, as illustrated in Fig. 1. A 9.5 kW reluctance synchronous machine (RSM) driven by another two-level VSI is employed to emulate the variable-speed wind turbine dynamics. Usually, the mechanical speed of the rotor ω_{m} is controlled by the PMSG to realize the MPPT of the wind turbine. Since the nonlinear speed controller $T_{\mathrm{e}}^{*} = -k_{\mathrm{p}}^{\star}\omega_{\mathrm{m}}^{2}$ is a slow controller, in this study, to test the dynamic performance of the proposed PLL, a fast speed controller is implemented for the RSM. The RSM is controlled using a nonlinear current PI-based FOC technique [25]. The two machines (i.e., PMSG and RSM) are coupled through a torque sensor as illustrated in Fig. 5. The control system of the PMSG and the proposed PLL are implemented in MATLAB/Simulink as shown in Fig. 1 and downloaded to a dSPACE DS1007 real-time platform via the Control Desk software. The switching frequencies of the power converters, as well as the sampling frequency, are set to 4 kHz with a dead-time period of 1 μs. The experimental setup is depicted in Fig. 5. The parameters of the PMSG are listed in Table 1.

Table 1 PMSG parameters

Name	Symbol	Value
Rated power	p_{rated}	14.5 kW
Rated stator line–line voltage	$u_{\mathrm{s,rated}}$	400 V
DC-link voltage	u_{dc}	560 V
Rated mechanical angular speed	$\omega_{\mathrm{m,rated}}$	209 rad/s
Stator resistance	R_{s}	0.15 Ω
Stator inductance	L_{s}	3.4 mH
Permanent-magnet flux linkage	ψ_{pm}	0.3753 Wb
Pole pairs	n_{p}	3

For comparison purposes, an incremental encoder with 2048 pulses per revolution (ppr) is used to measure the actual rotor position of the PMSG, which is fed to dSPACE using a DS3002 incremental encoder board. Three current sensors and one voltage sensor are used to measure the stator currents of the PMSG and the DC-link voltage, respectively. The measured currents and voltage are handed over to dSPACE through a DS2004 analog-to-digital converter (A/D) board. The reference voltage signals ($u_{\mathrm{s,ref}}^{\alpha}$, $u_{\mathrm{s,ref}}^{\beta}$) are used for the PLL instead of the real signals (u_{s}^{α}, u_{s}^{β}). A SVM is adopted to generate the respective switching signals of the power converters according to the demanded reference voltages. The power converters are controlled by dSPACE through a DS5101 pulse-width modulation board.

Generally, the performance of the speed and position observers for surface-mounted PMSG are challenging at low sampling rates and/or very low (i.e., approaching zero) speeds owing to the rotor isotropy which may lead to an unobservable system [26]. Fortunately, variable-speed wind turbines operate only when the wind speed is higher than a positive cut-in wind speed [6]. Consequently, zero speed is not within the discussed operation range. In this paper, the mechanical speed operation range is selected from 4 to 100 rad/s in order to present the performance of the proposed observer during low and medium speeds. The torque command of the PMSG is calculated as $T_{\mathrm{e}}^{\star} = -0.0061\hat{\omega}_{\mathrm{m}}^{2}$ with the positive gain $k_{\mathrm{p}}^{\star} = 0.0061$. This value of $k_{\mathrm{p}}^{\star}$ is selected in order to generate the rated mechanical torque of the RSM (i.e., $T_{RSM}^{rated} = 61\,\mathrm{N\,m}$) at the selected speed limit (here 100 rad/s). Therefore, any variation in the rotor speed of the PMSG will be followed with a variation in the generated power.

Figure 6 shows the dynamic response of the proposed PLL under step changes in the reference mechanical speed $\omega_{\mathrm{m,ref}}$ of the RSM from 10 to 60 rad/s, and then to 30 rad/s at the time instants $t = 4$ s and $t = 5$ s, respectively. According to Fig. 6, the proposed PLL tracks the rotor speed and position with a good dynamic and steady-state performance. Speed and position estimation errors (i.e., $\Delta\omega_{\mathrm{r}}$ and $\Delta\phi_{\mathrm{r}}$) converge

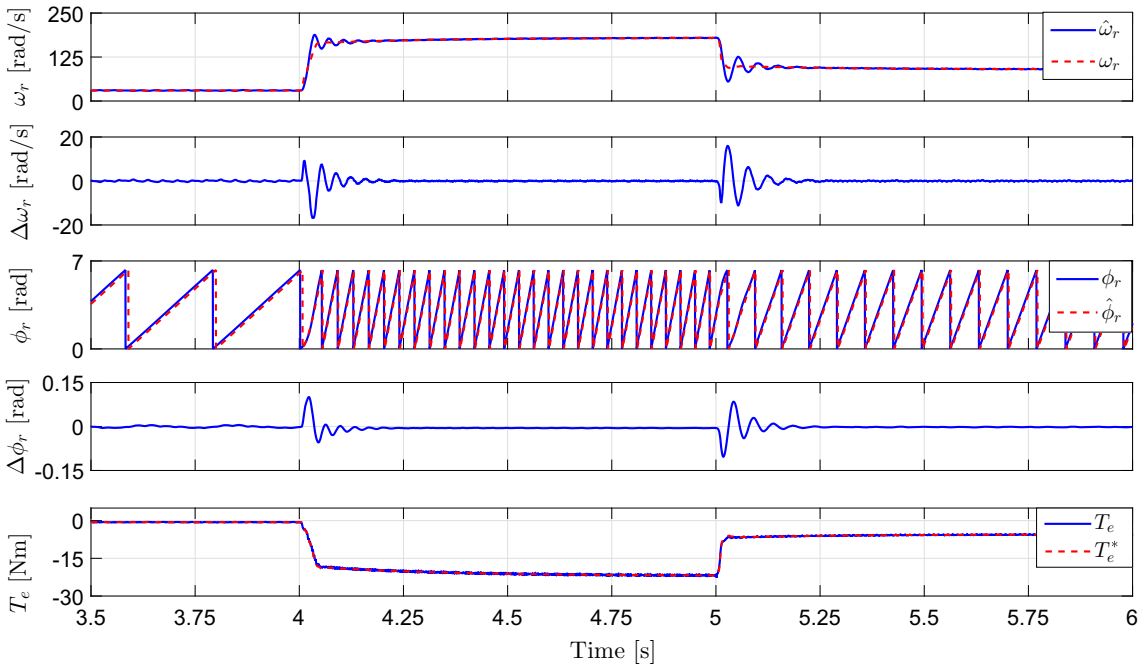

Fig. 6 Experimental results for step change in the rotor speed (from *top* to *bottom*): estimated $\hat{\omega}_\mathrm{r}$ and actual ω_r speed of the rotor, speed estimation error $\Delta\omega_\mathrm{r} = \omega_\mathrm{r} - \hat{\omega}_\mathrm{r}$, estimated $\hat{\phi}_\mathrm{r}$ and actual ϕ_r position of the rotor, position estimation error $\Delta\phi_\mathrm{r} = \phi_\mathrm{r} - \hat{\phi}_\mathrm{r}$, actual T_e and reference T_e^* torque

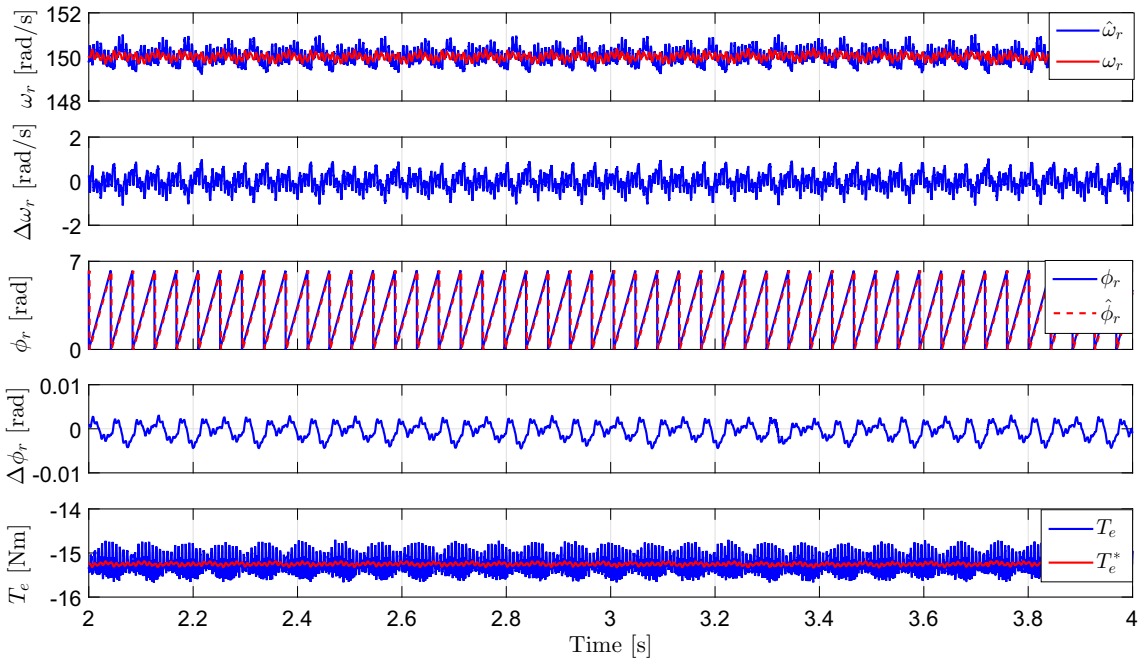

Fig. 7 Experimental results at steady-state (from *top* to *bottom*): estimated $\hat{\omega}_\mathrm{r}$ and actual ω_r speed of the rotor, speed estimation error $\Delta\omega_\mathrm{r} = \omega_\mathrm{r} - \hat{\omega}_\mathrm{r}$, estimated $\hat{\phi}_\mathrm{r}$ and actual ϕ_r position of the rotor, position estimation error $\Delta\phi_\mathrm{r} = \phi_\mathrm{r} - \hat{\phi}_\mathrm{r}$, actual T_e and reference T_e^* torque

quickly to zero, respectively. As shown in Fig. 6, the reference torque T_e^* is computed according to the rotor speed. Therefore, any change in the rotor speed induces a change in the generated electro-magnetic torque T_e and, hence, a change in the generated active power. This fact emulates variable-speed wind turbine systems in a realistic manner.

In order to further investigate the performance of the proposed PLL, the steady-state performance is illustrated

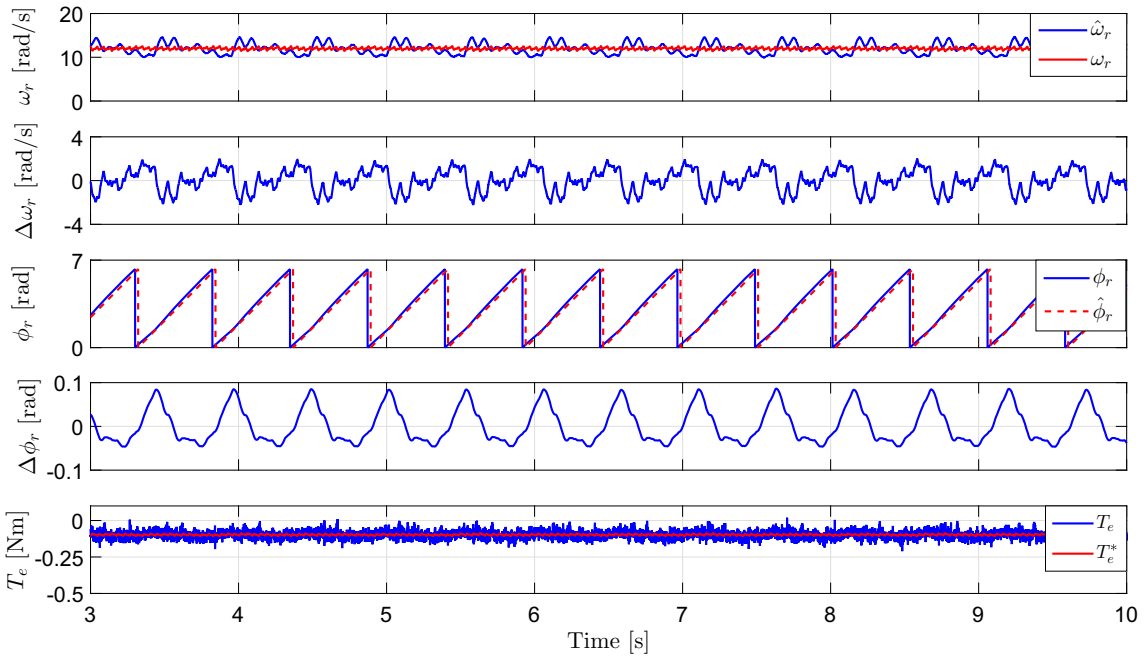

Fig. 8 Experimental results at the selected minimum speed (from *top* to *bottom*): estimated $\hat{\omega}_\mathrm{r}$ and actual ω_r speed of the rotor, speed estimation error $\Delta\omega_\mathrm{r} = \omega_\mathrm{r} - \hat{\omega}_\mathrm{r}$, estimated $\hat{\phi}_\mathrm{r}$ and actual ϕ_r position of the rotor, position estimation error $\Delta\phi_\mathrm{r} = \phi_\mathrm{r} - \hat{\phi}_\mathrm{r}$, actual T_e and reference T_e^* torque

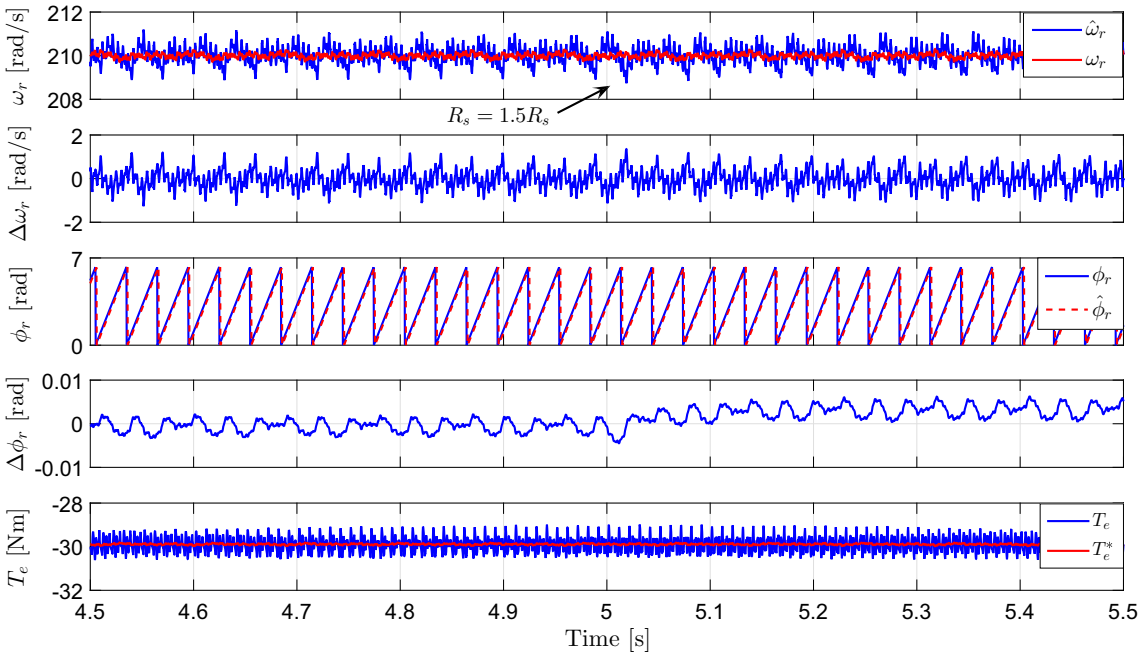

Fig. 9 Experimental results for a step change in the stator resistance R_s (from *top* to *bottom*): estimated $\hat{\omega}_\mathrm{r}$ and actual ω_r speed of the rotor, speed estimation error $\Delta\omega_\mathrm{r} = \omega_\mathrm{r} - \hat{\omega}_\mathrm{r}$, estimated $\hat{\phi}_\mathrm{r}$ and actual ϕ_r position of the rotor, position estimation error $\Delta\phi_\mathrm{r} = \phi_\mathrm{r} - \hat{\phi}_\mathrm{r}$, actual T_e and reference T_e^* torque

in Fig. 7. The mechanical speed ω_m of the rotor is set to 50 rad/s by the RSM control system. It can be observed that the proposed PLL gives an accurate steady-state estimation response. The speed and position estimation errors (i.e., $\Delta\omega_\mathrm{r}$ and $\Delta\phi_\mathrm{r}$) are almost zero, respectively.

Moreover, the performance of the proposed PLL at the selected minimum speed (i.e., $\omega_\mathrm{m} = 4$ rad/s) is investigated. According to Fig. 8, the proposed PLL gives a good estimation response at the selected minimum speed. The speed and position estimation errors (i.e., $\Delta\omega_\mathrm{r}$ and $\Delta\phi_\mathrm{r}$) are small.

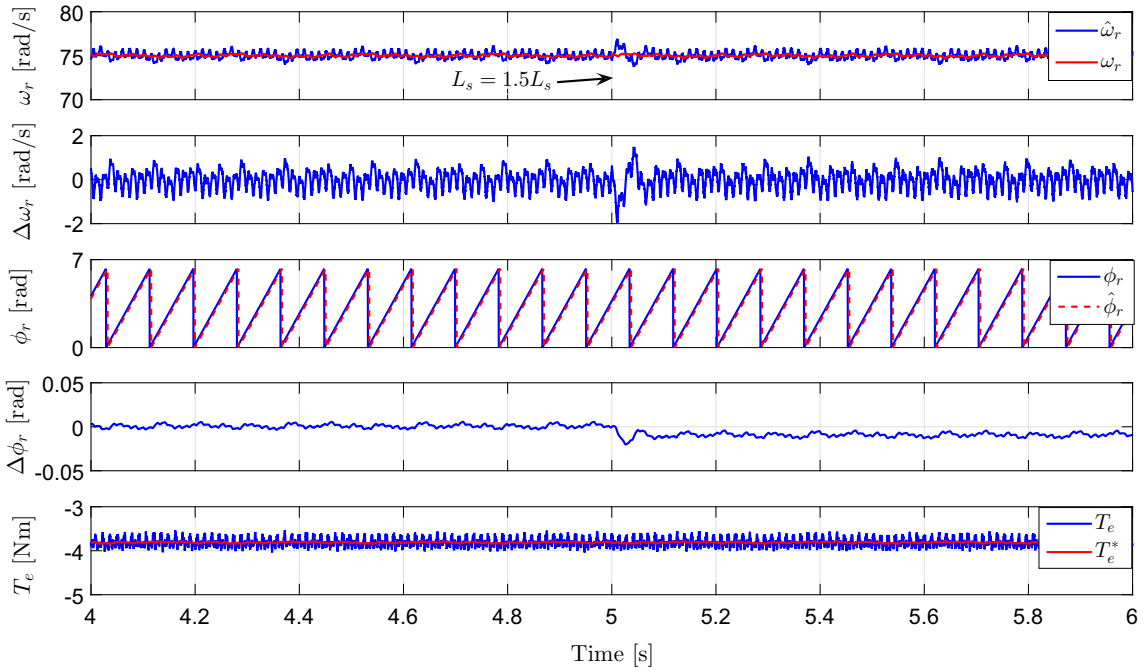

Fig. 10 Experimental results for a step change in the stator inductance L_s (from *top* to *bottom*): estimated $\hat{\omega}_\mathrm{r}$ and actual ω_r speed of the rotor, speed estimation error $\Delta\omega_\mathrm{r} = \omega_\mathrm{r} - \hat{\omega}_\mathrm{r}$, estimated $\hat{\phi}_\mathrm{r}$ and actual ϕ_r position of the rotor, position estimation error $\Delta\phi_\mathrm{r} = \phi_\mathrm{r} - \hat{\phi}_\mathrm{r}$, actual T_e and reference T_e^* torque

The parameter sensitivity of the proposed PLL is also investigated. Figure 9 shows the response of the proposed PLL at 50% step change in stator resistance R_s within the real-time model. The mechanical speed ω_m of the rotor is set to 70 rad/s by the RSM control system. As can be seen, the variation of stator resistance R_s has a very small impact on the performance of the proposed PLL. A very small deviation in the estimated position of the rotor was produced because of the stator resistance R_s variation.

Furthermore, the robustness with respect to changes (due to magnetic saturation) in the stator inductance L_s is investigated. Therefore, L_s is increased by 50% at the time instant $t = 5\,\mathrm{s}$. The mechanical speed ω_m of the rotor is set to 25 rad/s by the RSM control system. Figure 10 illustrates the experimental results of the proposed PLL for this scenario. Again, the proposed PLL shows an accurate estimation performance and acceptable robustness against parameter uncertainties also in L_s. Only, small deviations in the estimated speed and position occur due to the inductance variation.

5 Conclusion

In this paper, a sensorless field-oriented control strategy for permanent-magnet synchronous generators in variable-speed wind turbine systems was proposed. The proposed method is based on a synchronously rotating reference frame phase-locked loop that utilizes a model-based back electromotive force to estimate the rotor speed and position of the permanent-magnet synchronous generator. The proposed strategy has been experimentally validated. The experimental results have shown that the proposed phase-locked loop tracks rotor speed and position with high accuracy. Furthermore, the proposed phase-locked loop is relatively robust to variations of the stator resistance and inductance of the permanent-magnet synchronous generator.

References

1. Liserre M, Cardenas R, Molinas M, Rodriguez J (2011) Overview of multi-MW wind turbines and wind parks. IEEE Trans. Ind Electron 58(4):1081–1095
2. Jeong HG, Lee KB (2014) A control scheme to fulfill the grid-code under various fault conditions in the grid-connected wind turbines. Electr Eng J 96(2):199–210
3. Abdelrahem M, Kennel R (2016) Fault-ride through strategy for permanent-magnet synchronous generators in variable-speed wind turbines. Energies 9(12):1–15
4. Abdel-Salam M, Ahmed A, Abdel-Sater M (2011) Harmonic mitigation, maximum power point tracking and dynamic performance of variable speed grid connected wind turbine. J Electr Power Compon Syst 39(2):176–190
5. Zhang Z, Hackl C, Abdelrahem M, Kennel R (2016) Voltage sensorless direct model predictive control of 3L-NPC back-to-back power converter PMSG wind turbine systems with fast dynamics. In: Proceedings of power and energy student summit (PESS 2016)

6. Zhao Y, Wei C, Zhang Z, Qiao W (2013) A review on position/speed sensorless control for permanent-magnet synchronous machine-based wind energy conversion systems. IEEE J Emerg Sel Topics Power Electron 1(4):203–216
7. Benadja M, Chandra A (2015) Adaptive sensorless control of PMSGs-based offshore wind farm and VSC-HVdc stations. IEEE J Emerg Sel Topics Power Electron 3(4):918–931
8. Abdelrahem M, Hackl C, Kennel R (2017) Simplified model predictive current control without mechanical sensors for variable-speed wind energy conversion systems. Electr Eng J 99(1):367–377
9. Abdelrahem M, Hackl C, Zhang Z, Kennel R (2016) Sensorless control of permanent magnet synchronous generators in variable-speed wind turbine systems. In: Proceedings of power and energy student summit (PESS 2016), Aachen, Germany, 19–20 January 2016
10. Rigatos G, Siano P, Zervos N (2014) Sensorless control of distributed power generators with the derivative-free nonlinear Kalman filter. IEEE Trans Ind Electron 61(11):6369–6382
11. Yan J, Lin H, Feng Y, Guo X, Huang Y, Zhu ZQ (2013) Improved sliding mode model reference adaptive system speed observer for fuzzy control of direct-drive permanent magnet synchronous generator wind power generation system. IET Renew Power Gener 7(1):28–35
12. Abdelrahem M, Hackl C, Kennel R (2016) Model predictive control of permanent magnet synchronous generators in variable-speed wind turbine systems. In: Proceedings of power and energy student summit (PESS 2016), Aachen, Germany, 19–20 January 2016
13. Liu W, Chen L, Ou J, Cheng S (2011) Simulation of PMSG wind turbine system with sensor-less control technology based on model reference adaptive system. In: International conference on electrical machines and systems, Beijing, 2011, pp. 1–3
14. Zhang Z, Zhao Y, Qiao W, Qu L (2014) A space-vector-modulated sensorless direct-torque control for direct-drive PMSG wind turbines. IEEE Trans Ind Appl 50(4):2331–2341 July-Aug. 2014
15. Koch G, Gabbi T, Henz G, Vieira RP, Pinheiro H (2015) Sensorless technique applied to PMSG of WECS using sliding mode observer. In: IEEE 13th Brazilian power electronics conference and 1st southern power electronics conference (COBEP/SPEC), Fortaleza, 2015, pp. 1–6
16. Huang K, Zheng L, Huang S, Xiao L, Li W (2011) Sensorless control for direct-drive PMSG wind turbines based on sliding mode observer. In: International conference on electrical machines and systems, Beijing, pp. 1–5
17. Hui Li, Shi KL, McLaren PG (2005) Neural-network-based sensorless maximum wind energy capture with compensated power coefficient. IEEE Trans Ind Appl 41(6):1548–1556
18. Singh M, Chandra A (2011) Application of adaptive network-based fuzzy inference system for sensorless control of PMSG-based wind turbine with nonlinear-load-compensation capabilities. IEEE Trans Power Electron 26(1):165–175
19. Golestan S, Guerrero JM, Vasquez JC (2017) Three-phase PLLs: a review of recent advances. IEEE Trans Power Electron 32(3):1894–1907
20. Comanescu M, Xu L (2006) An improved flux observer based on PLL frequency estimator for sensorless vector control of induction motors. IEEE Trans Ind Electron 53(1):50–56
21. Preindl M, Schaltz E (2011) Sensorless model predictive direct current control using novel second-order PLL observer for PMSM drive systems. IEEE Trans Ind Electron 58(9):4087–4095
22. Tong L et al (2014) An SRF-PLL-based sensorless vector control using the predictive deadbeat algorithm for the direct-driven permanent magnet synchronous generator. IEEE Trans Power Electron 29(6):2837–2849
23. Fan S, Wang P, Wen C (2010) A new sensorless control strategy used in direct-drive PMSG wind power system. In: 2nd international symposium on power electronics for distributed generation systems. China, Hefei, pp 611–615
24. Dirscherl C, Hackl C, Schechner K (2015) Modellierung und Regelung von modernen Windkraftanlagen: Eine Einführung" (Chapter 24). In: Schröder D (ed) Elektrische Antriebe - Regelung von Antriebssystemen. Springer, New York, pp 1540–1614
25. Hackl C, Kamper M, Kullick J, Mitchel J (2016) Current control of reluctance synchronous machines with online adjustment of the controller parameters. In: Proceedings of the 2016 IEEE international symposium on industrial electronics (ISIE 2016), Santa Clara, USA, p. 153–160,
26. Shi T, Wang Z, Xia C (2015) Speed measurement error suppression for PMSM control system using self-adaption Kalman observer. IEEE Trans Ind Electron 62(5):2753–2763